Analysis of the impact resistance of adhesively bonded, curved polycarbonate windshields

Lars Bühler, Stefan Andreas Ritt, Dorothea Schlie, Nathalie Toso, Heinz Voggenreiter, German Aerospace Center (DLR), Stuttgart, Germany
Matthias Tretter, Patrick Kronhofmann, Enkhchuluun Leege, KRD Luftfahrttechnik, Geesthacht, Germany

Abstract

Polycarbonate windshields have superior impact properties but deform significantly during impact. In this paper, the deformation during impact with a soft impactor was measured and compared to simulation results. A cylindrical windshield with a length of 1400 mm and a radius of 460 mm, derived from a real geometry, was impacted with an artificial bird at 65 m/s. To measure the full-field deformation in the impact area, a film with a printed speckle pattern was applied on the windshield and 3D Digital Image Correlation (DIC) was used. The finite element simulations were performed in LS-DYNA. To enable a comparison of the deformations, the subset midpoints of the DIC results were used as history nodes in the simulation. This method facilitated the identification of regions that exhibited varying degrees of deformation and enabled both qualitative and quantitative comparisons to be made.

1. NOTATION

Acronyms:	
DIC	Digital Image Correlation
ERF	European Rotorcraft Forum
PC	Polycarbonate
VTOL	Vertical Take-Off and Landing

2. INTRODUCTION

Bird strikes pose a significant threat to aviation safety (Ref. *1*). The likelihood of a bird strike decreases consistently with increasing altitude, making rotorcraft particularly susceptible due to their specific flight altitudes (Ref. *2, 3*). The majority of bird strikes on rotorcraft occur on components forward of the main rotor mast, with the windshield being the most frequently affected (Ref *2, 3*). As a result, bird strike protection is mandatory for windshields of newly certified rotorcrafts with six or more passengers (Ref. *4, 5*), as well as for vertical take-off and landing (VTOL)-capable aircraft (Ref. *6, 7*).

In recent years, polycarbonate windshields have been increasingly used to improve impact resistance while minimizing weight (Refs. *8–12*). Although polycarbonate offers superior impact resistance compared to acrylic glass, it can deform significantly under impact loading, potentially leading to increased stress in the adjacent structures (Ref. *13*). Several studies have used different techniques to measure these deformations. For instance, Plassard (Ref. *14*) used Photonic Doppler Velocimetry (PDV) to measure the displacement of the impact point during bird strikes on flat, angled polycarbonate plates. Ćwiklak (Ref. *15*) recorded the displacement during bird impacts on both flat and curved polycarbonate surfaces at specific points using a camera. The DIC method has already been used by Ritt (Ref. *16*) to measure the deformation over a large area during hard and soft body impacts on an adhesively bonded, flat polycarbonate windshield. Additionally, Dadouche (Ref. *17*) employed 3D DIC to measure deformation during the impact of a drone on a flat aluminium plate. Beyond displacement measurement, Mohagheghian (Ref. *18, 19*) also quantified the strains during the impact of an artificial bird on a flat, laminated windshield and compared the results with simulation data.

In this study, the method of measuring deformations with 3D DIC during impact is transferred to curved windshields in the shape of a cylinder segment. An adhesively bonded windshield demonstrator was developed based on a representative geometry and experimentally tested to analyze the bird strike resistance. For the evaluation, the novel approach depicted in Figure 1 was used. The deformation results from DIC were exported and transformed into a reference coordinate. The subset center points were used as history nodes in the simulation, which allowed for tracking and comparing the displacement at each specific node between experiment and simulation.

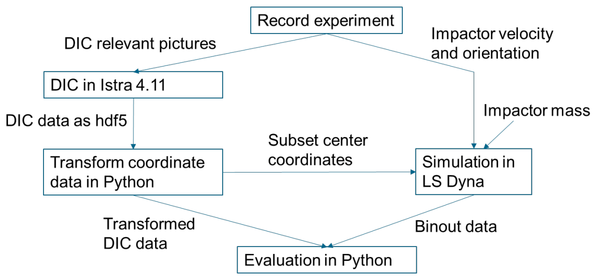

Figure 1: Evaluation of Test and Experiment

3. METHODS

3.1. Experimental setup

The demonstrator (see Figure 2) was developed to evaluate the impact properties of different design concepts. To facilitate the manufacturing of the windshield and the test rig, the complex target geometry was simplified to a single curved shape with straight edges. The dimensions of the demonstrator – length, radius, width, and thickness – were derived based on a central impact scenario.

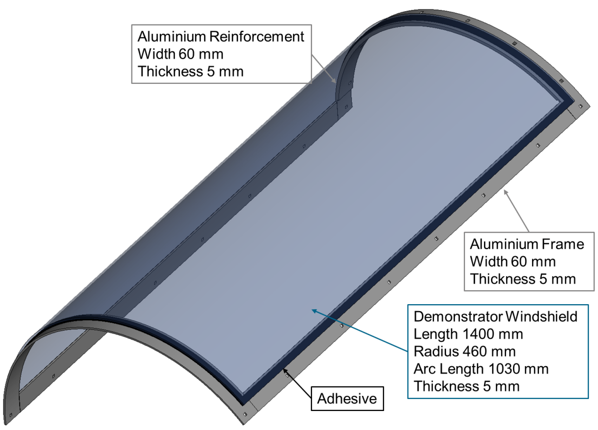

Figure 2: Demonstrator

Compared to the real case scenario, the structure is rotated by 90 degrees around the impact axis of the test (see Figure 3). This allowed for easy modification of the impact position and angle, providing flexibility in testing various conditions. Nevertheless, an impact angle of 33° was used throughout this paper, derived from the reference load case. The aluminum frame of the demonstrator is connected to a supporting structure made of steel, which itself is attached to two steel beams. The setup enabled capturing the impact area with two cameras and thus the evaluation via 3D DIC. Additional cameras were used to measure the velocity of the impactor and for a nearly frontal and top view of the impact (see Figure 4). The figure also shows the coordinate systems used: in all of them, the origin is at the theoretical impact point. The xy-plane is parallel to the ground, and the z-axis points upward. In the test and simulation coordinate system (x, y, z), the x-axis represents the impact direction. The analysis coordinate system (x', y', z') is rotated by the impact angle so that the x'-axis runs parallel to the demonstrator.

Figure 3: Experimental setup without speckle film

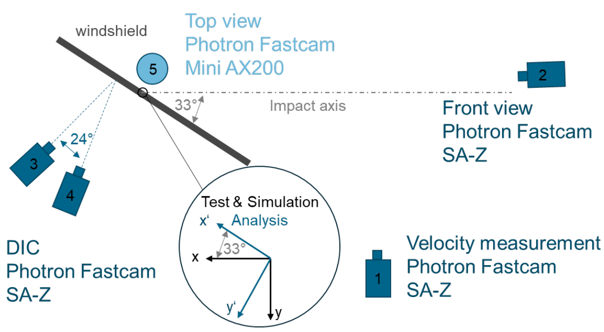

Figure 4: Camera positions and used coordinate systems

As impact load case, a soft projectile of 1.0 kg mass was applied. This artificial bird (named DLRRAB and shown in Ref. *20*) in an ellipsoidal shape was accelerated to a target velocity of 64 m/s using a 200 mm gas gun with a 12 m barrel length.

The details of the DIC setup are listed in Table *1*. A foil with a printed pattern was used to create the speckles. Applying this foil precisely to the inside of the curved windshield proved challenging, with minor imperfections such as air bubbles and folds occasionally occurring. In contrast to Ref. *16*, no shadows from the impactor affected the measurement, eliminating the need for additional painting of the front as discussed in Ref. *18*.

The evaluation was performed with the software Istra 4.11.1 by Dantec Dynamics. A Gaussian filter was applied to mitigate potential aliasing effects from feature sizes smaller than 3 pixels. For a simplified noise floor analysis, the time steps before the impact (approx. 30 ms) were analysed. The maximum displacement was in the order of 1 mm, the maximum strain in the order of 0.04.

Table 1: DIC Hardware and Analysis Parameters

Parameter	Value
Camera	Photron Fastcam SA-Z
Stereo-Angle	~ 24°
Image scale	~ 1 px/mm
Image Acquisition Rate	10,000 fps
Patterning Technique	Adhesive foil
Pattern Feature Size	~ 3 mm
Software	Istra4D 4.11.1 (Dantec Dynamics)
Subset Size	19 x 19 px
Step Size	14 px
Image Filtering	Gaussian low pass filter (sigma 0.3 px)
Subset Shape Function	Bilinear
Noise floor	Displacement ~ 1 mm True eff. strain ~ 0.04

3.2. Numerical model

Numerical simulations were performed using the explicit solver LS-DYNA (version 15.0.2) in double precision in MPP on a Linux system. The model of the demonstrator used in the simulation is shown in Figure 5. The vertical beams were not modeled. Instead, all nodes of the support structure in contact with the beams were fixed to represent their constraints. The bolt connections between the aluminum frame and the steel support structure were modeled using beam elements (*SECTION_BEAM) with spot weld material properties (*MAT_SPOTWELD). Therefore, the center points of the holes were created as *CONSTRAINED_NODAL_RIGID_BODY. During a dynamic relaxation phase, the bolts were preloaded to close the gap between the two structures, resulting in minor deformations and strains in the windshield. The points from DIC were used as history nodes. For this purpose, they were tied to the inner windshield surface using an increased contact distance SAST.

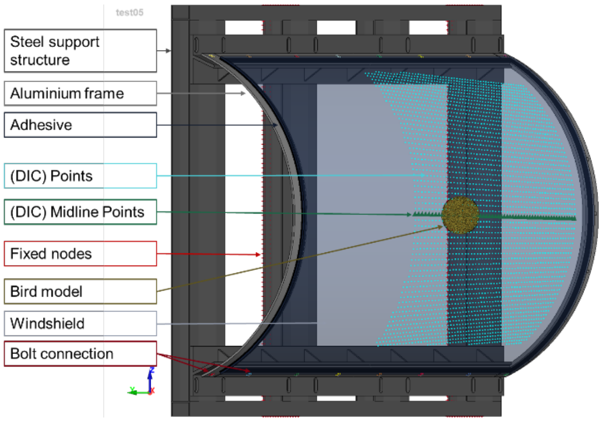

Figure 5: Simulation model

Details of the impactor and windshield models were presented in Ref. *21*. The used material models in the demonstrator are summarized in Table *2*. The artificial bird was modeled with approx. 25,000 SPH particles with a close to identical particle distance as proposed in Ref *22*. The hull was modeled with shell elements that were significantly thinner than in the experimental bird.

Table 2: Demonstrator material models

Parameter	Value
Material model (PC)	*MAT_187L (+Gissmo)
Elastic modulus (PC)	2.35 GPa
Material model (Adhesive)	*MAT_240
Material model (Alu)	*MAT_024
Elastic modulus (Alu)	68.04 GPa
Material model (Steel)	*MAT_001
Elastic modulus (Steel)	210.00 GPa

4. RESULTS AND DISCUSSION

4.1. Experimental results

Table *3* provides an overview of the performed tests. Only test02 and test05 will be discussed in more detail, as full-field DIC results are available. In both tests, no failure of the windshield or the adhesive was observed.

Table 3: Test data and results

Test	Mass [kg]	Velocity [m/s]	Max. displacement [mm]
01	1.053	65.0	145.6[a]
02	1.058	65.0	139.2
03	1.059	65.6	143.7[b]
04	1.059	66.7	144.1[b]
05	1.061	64.5	144.3
06	1.059	64.5	137.8[c]

[a] no Aluminium reinforcement was used

[b] Using two DIC foils with a joint in the impact area caused failure and detachment

[c] use of old DIC foil led to reflections

The impact time was initially determined based on the images from camera5. Subsequent analysis of the results, however, suggested that the DIC cameras were not perfectly synchronized in time with camera5. As a result, the DIC measurements lagged behind the simulation data. For example, the impact became visible in the experimental data after approximately 0.5 ms, whereas it occurred after approximately 0.2 ms in the simulation. Consequently, the timing in the deformation measurements was adjusted based on the onset of the first visible deformation.

When properly used, the speckle foil remained in place and enabled a successful evaluation by DIC. In two tests, instead of using a single continuous film, two separate films were applied with a seam located in the impact area. This configuration led to adhesive failure and tears at the joint. Additionally, in one case, the use of an old foil (as used in Ref. *16*) led to reflections and large areas not analysable. The correlation software Istra4D was able to track the subsets in the impact area throughout the tests. However, in the boundary regions, the subsets were partly not or not correctly identified.

The simplified noise floor analysis indicates a high level of uncertainty. The deformation error of 1 mm corresponds to less than 1% of the maximum deformation and is therefore acceptable. However, the error in strain measurement is comparable to the strain values themselves, posing a significant concern about the validity. Several approaches could contribute to improving the measurement. Redesigning the support structure and optimizing the positioning of the beams to expand the field of view and enhance lighting conditions may be particularly beneficial for measurements in the peripheral regions. Introducing a Central Reference Camera Perspective (CRCP) by integrating a third camera could also improve the coverage of the peripheral areas while simultaneously enhancing measurement accuracy, as suggested in Ref. *23*. Furthermore, using the recommended feature size of 3-5 px and reducing the exposure time to minimize motion blur may contribute to improved measurement accuracy (see Ref. *24*).

Figure 6 shows the impact event in test05. The reinforcement of the artificial bird shattered upon impact and the soft projectile “flowed” along the windshield. The windshield deflected strongly but returned to its original shape after impact. After the test, only traces of the impactor, but no plastic deformation, can be seen on the windshield.

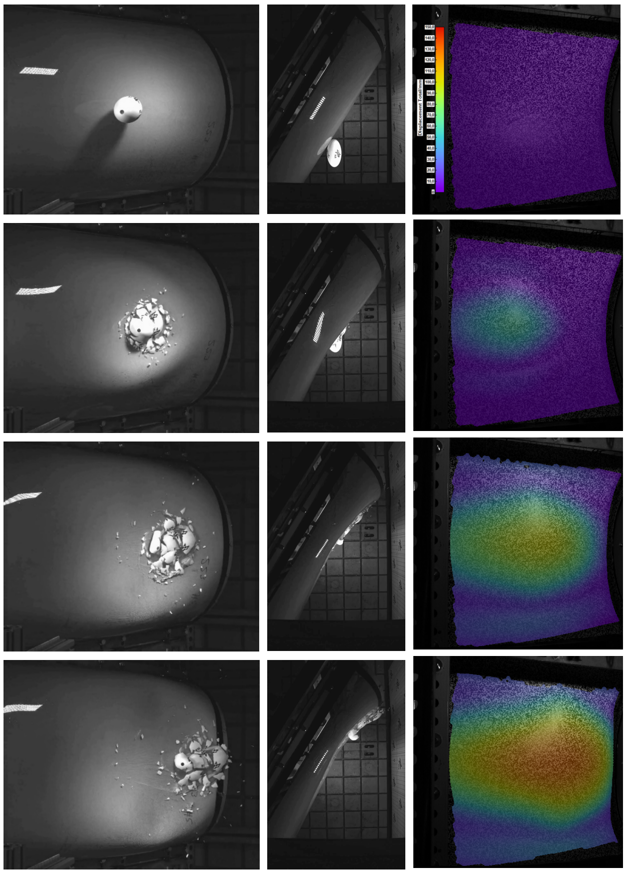

Figure 6: Camera pictures during test05 from camera 2, 4 and 5 at times 0 ms, 4 ms, 8 ms and 12 ms (t=0 ms from camera 5)

The results of the strain measurement using DIC were not analysed in detail due to the measurement inaccuracy. The data was transformed into the analysis coordinate system and analyzed in Python. The deformation in all tests is shown in the appendix (see

Figure 13). This paper focuses on the results from test02 and test05. The deformation in these tests at different times is shown in Figure 7. The difference between the deformations in both tests is also shown, with a positive value indicating greater deformation in test05. Since the impact mass and velocity are almost identical, other factors (impact point and impactor orientation, different adhesives, etc.) are the main reasons for the differences.

A more detailed view of the deformation at the center line is given in Figure 8. The difference between the two tests increases over time until it decreases at the end of the rebounding phase. This is related to a longer displacing phase and a delayed rebounding phase in test05.

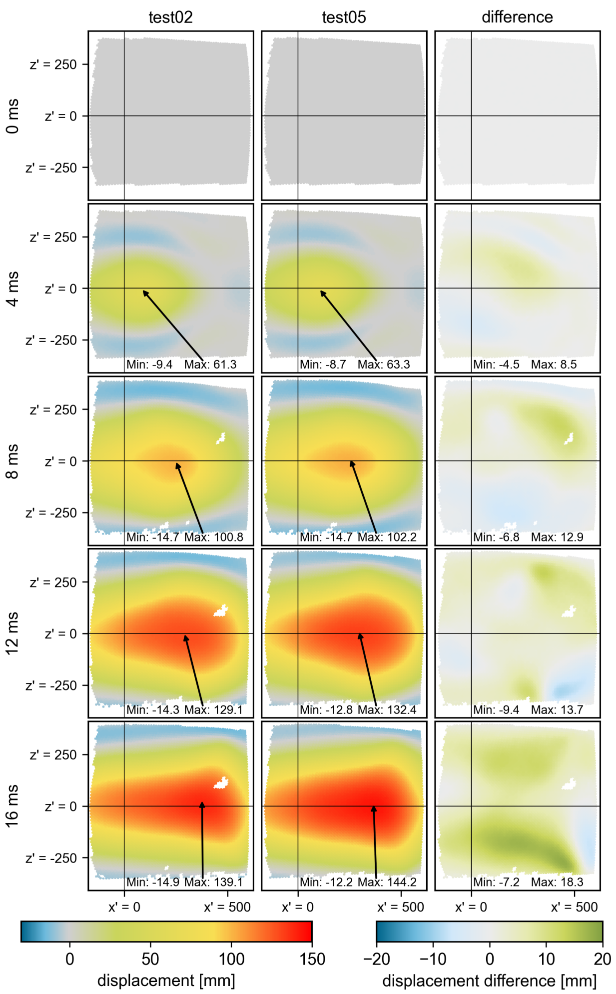

Figure 7: y' displacement of the surface over time for test02 and test05 and the resulting difference

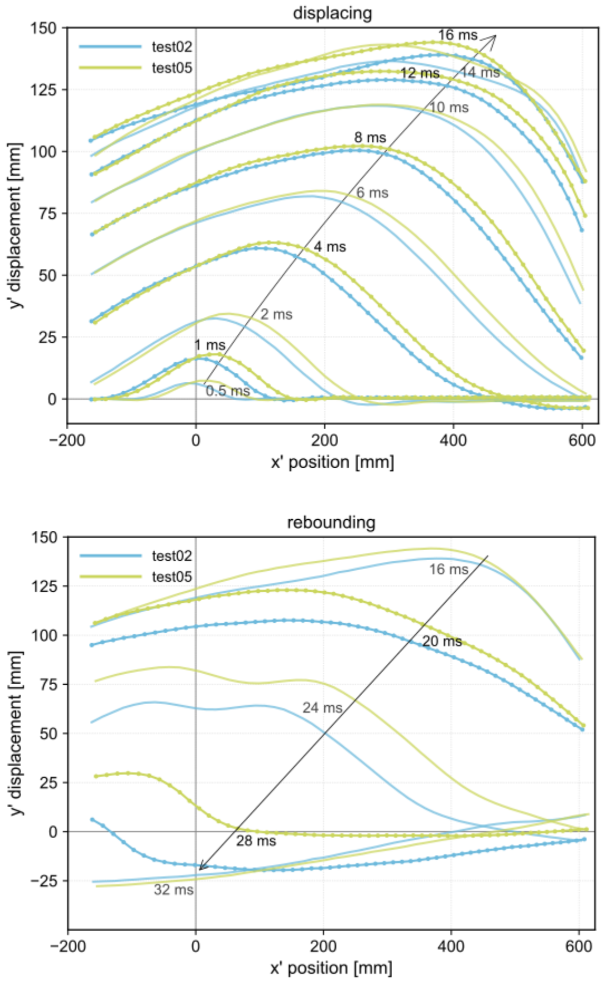

Figure 8: y' displacement on the midline over time for test02 and test05 (top: displacing, bottom: rebounding)

4.2. Numerical results and comparison to experiments

In the simulation, the parameters of test05 (see Table 3) were used. Due to noise in the experimental data, the strains in the simulation are shown here without a comparison to the test data. The maximum effective strain is approximately 3 %, which is far from the elongation at break of polycarbonate (> 50 %). In Figure 9 the effective strain in the windshield at 4 ms and 16 ms is plotted. An analysis of the prevailing triaxialities within the windshield revealed a complex stress distribution. Depending on the time and spatial location – not only across the surface but also across the thickness – different stress states occur. These range from compressive to shear and (uniaxial and biaxial) tensile stresses, illustrating the complex mechanical behavior. Additionally, the strain rates vary and temporarily reach up to 500 /s.

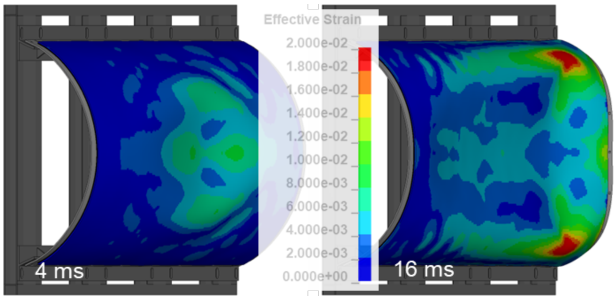

Figure 9: effective strain in the windshield at 4ms and 16 ms

The use of the facet midpoints allowed the correlation of the deformations to be assessed not only in terms of quality but also in terms of quantity. Figure 10 presents the displacement at different times and the deviation compared to the experimental results. Since the mass and velocity of test02 are nearly identical, also a comparison to this test was done. In addition, Figure 11 shows a comparison of the deformations at the center line with the two reference tests.

The advantages of the comparison method used are evident here: While deviations are barely noticeable in a purely visual comparison of the deformation fields (see Figure 7, Figure 10) and even the centerline comparison showes almost no discrepancies, the point-by-point comparison allows for clear identification of areas with larger deviations and the quantification of the deviation (see histogram in Figure 12). On the experimental side, inaccuracies in the DIC data (e.g., background noise, deviation in coordinate transformation) and general fluctuations between tests (such as between Test02 and Test05) are possible causes for deviations. On the simulation side, sources of error include slight deviations in the position of the history nodes (the DIC nodes were shifted in the Tied Contact so that they lay on the surface of the simulation geometry), deviations in the modeling of the impactor (hull not considered accuratly), the bonding (non-consideration of irregular bonding, use of a material card from a similar adhesive), and the windshield. In future works, the windshield material will be further analyzed to improve the understanding and simulation of the deformation and failure behavior (e.g., stress-state and strain rate dependency).

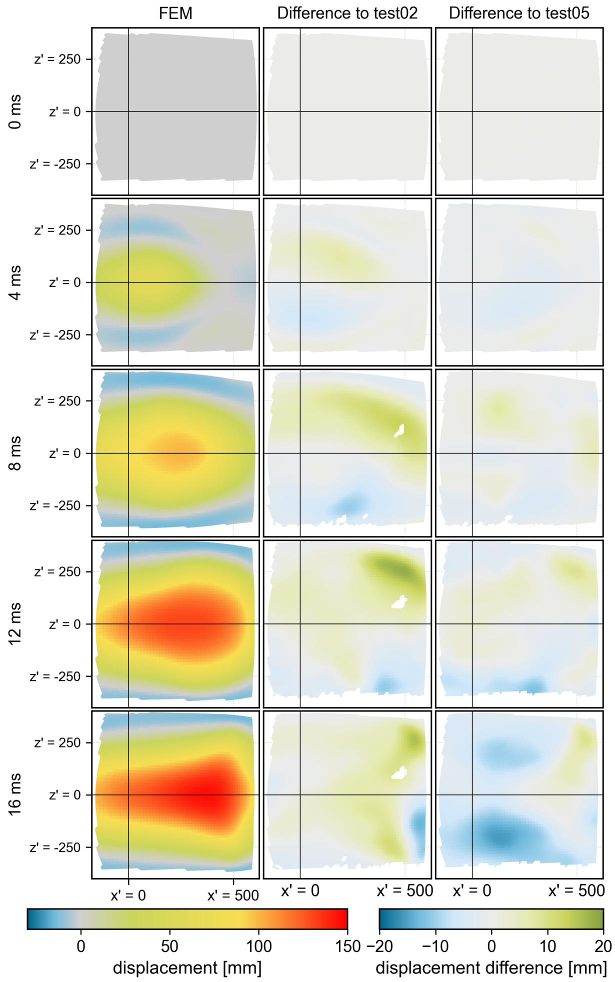

Figure 10: y' displacement of the surface over time for the simulation and difference to the reference tests

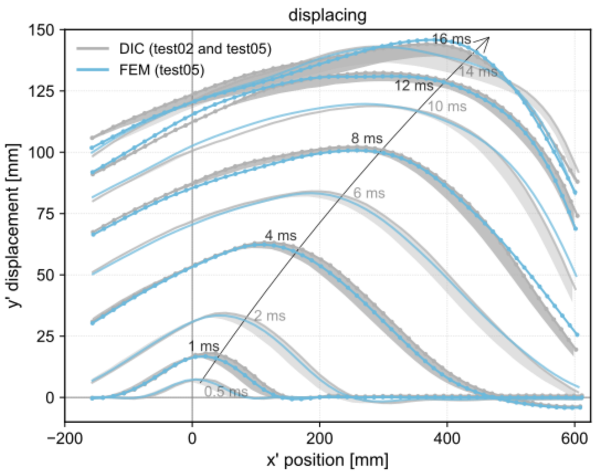

Figure 11: y' displacement on the midline over time for the simulation of test05 and comparison to DIC data

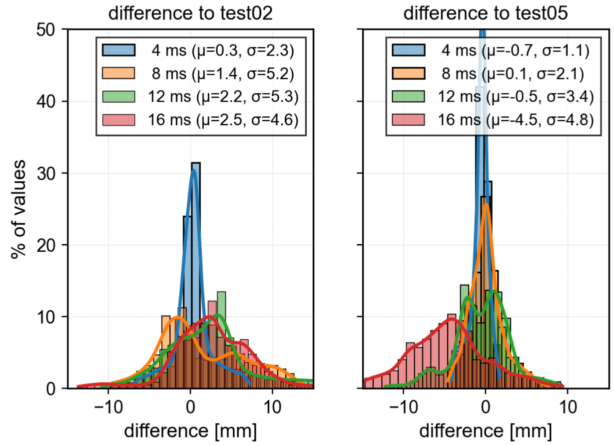

Figure 12: histogram of the y' displacement difference between the simulation and the reference tests

5. CONCLUSIONS

1. The use of 3D DIC with a glued speckle foil allowed the deformation measurement of a curved polycarbonate windshield during impact.
2. Using the facet midpoints enabled an easy qualitative and quantitative comparison between the deformations of different experiments and between experiment and simulation.
3. The deformation in the experiments and the simulations showed good agreement.
4. The DIC setup should be optimized in further experiments in order to reduce noise and enable precise strain measurement.
5. Further research is planned to better understand and simulate the deformation and failure behavior of polycarbonate.

Author contact:

Lars Bühler lars.buehler@dlr.de

Stefan Andreas Ritt Stefan-andreas.ritt@dlr.de

Matthias Tretter matthias.tretter@kasiglas.de

6. APPENDIX

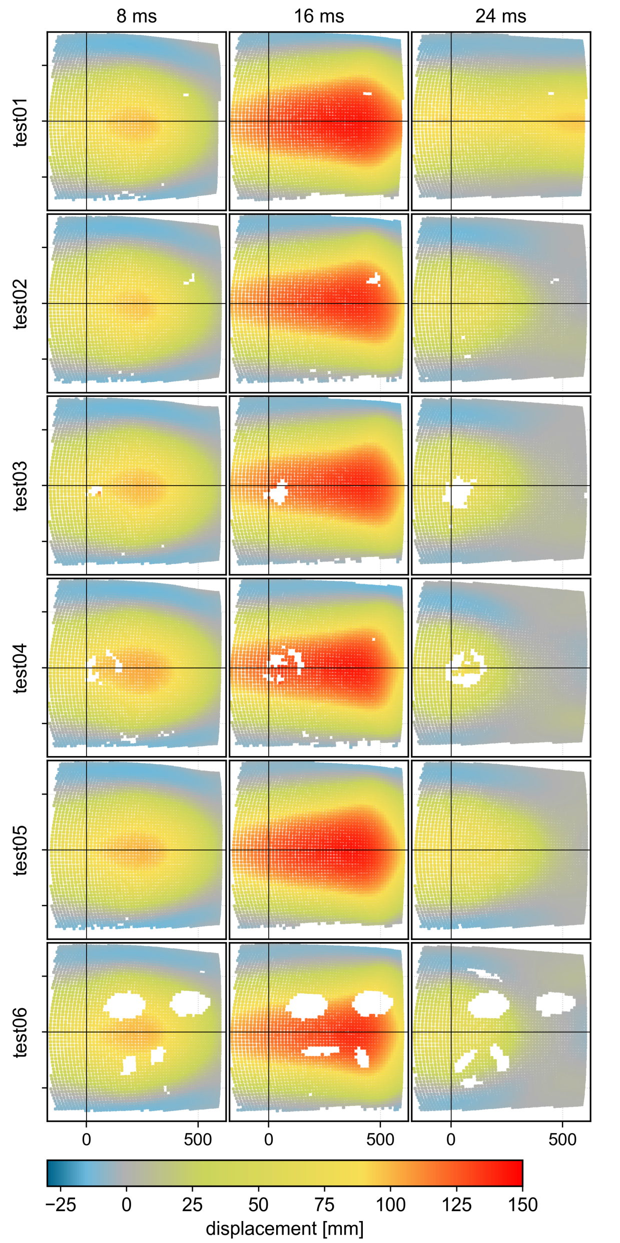

Figure 13: y' displacement of the surface over time for all tests

7. REFERENCES

1. DeVault, T. L., B. F. Blackwell, T. W. Seamans, M. J. Begier, J. D. Kougher, J. E. Washburn, P. R. Miller, and R. A. Dolbeer. Estimating Interspecific Economic Risk of Bird Strikes with Aircraft. *Wildlife Society Bulletin*, Vol. 42, No. 1, 2018, pp. 94–101 doi: 10.1002/wsb.859.
2. *Rotorcraft Bird Strike Working Group*. Recommendations to the Aviation Rulemaking

Advisory Committee (ARAC) Rev. B, ARAC, 2019. https://www.faa.gov/regulations_policies/rulemaking/committees/documents/media/ARAC%20RBSWG%20Final%20Report%20Rev.%20B.pdf.

3. Washburn, B. E., P. J. Cisar, and T. L. DeVault. Impact Locations and Damage to Civil and Military Rotary-Wing Aircraft from Wildlife Strikes, 2018 doi: 10.26077/6yvw-8k56.

4. *CS-27 Amendment 10*. Certification Specifications, Acceptable Means of Compliance and Guidance Material for Small Rotorcraft (CS-27), European Union Aviation Safety Agency (EASA), 2023.

5. *CS-29 Amendment 12*. Certification Specifications, Acceptable Means of Compliance and Guidance Material for Large Rotorcraft (CS-29), European Union Aviation Safety Agency (EASA), 2024.

6. *SC-VTOL-02*. Special Condition for Small-Category VTOL-Capable Aircraft. Issue 2, European Union Aviation Safety Agency (EASA), 2024.

7. 89 FR 17230. Airworthiness Criteria: Special Class Airworthiness Criteria for the Joby Aero, Inc. Model JAS4-1 Powered-Lift. Federal Aviation Administration (FAA). https://www.federalregister.gov/documents/2024/03/08/2024-04690/airworthiness-criteria-special-class-airworthiness-criteria-for-the-joby-aero-inc-model-jas4-1#print.

8. Aeronautical Accesories. *Bell Helicopter 407 and 206 Series Polycarbonate Windshield.* https://www.aero-access.com/products/Bell-407-Polycarbonate-Windshield-Replacement-Kit.html.

9. Aeronautical Accesories. *Bell Medium Polycarbonate Windshield.* https://aeroaccess.ebizcdn.com/media/AA%20Bell%20Medium%20Polycarbonate%20Windshield%20Brochure.pdf.

10. Robinson Helicopter. *Improved Bird Strike Protection*, 2020.

11. Robinson Helicopter Company. *Robinson Helicopter Company Shows Upgraded Version of the R66 NxG, at Verticon 2025 in Dallas*, 2025.

12. Sabic. *Leonardo Helicopters AW169 Windshield*, 2022. https://kshow.sabic.com/en/Images/SABIC-K2022-SC-T035-Helicopter-Final_tcm1030-37404.pdf.

13. *CS-25 Amendment 28*. Certification Specifications and Acceptable Means of Compliance for Large Aeroplanes (CS-25), European Union Aviation Safety Agency (EASA), 2023.

14. Plassard, F., P.-L. Hereil, P. Joseph, and J. Mespoulet. Experimental and Numerical Study of a Bird Strike Against a Windshield. *EPJ Web of Conferences*, Vol. 94, 2015, p. 1051 doi: 10.1051/epjconf/20159401051.

15. Ćwiklak, J., P. Gołda, A. Goś, E. Kobiałka, and K. Krasuski. Experimental and Numerical Investigations on Polycarbonate Samples and Rotorcraft Windshield for Bird Model Impacts. *Archives of Transport*, Vol. 70, No. 2, 2024, pp. 79–96 doi: 10.61089/aot2024.eea5zs04.

16. Ritt, S. A., and J. Oswald. Analysis of Hard and Soft Body Impact on Rotorcraft Windshields. *Aerospace Structural Impact Dynamics International Conference -ASIDIC 2019*, 2019.

17. Dadouche, A., A. Greer, B. Galeote, T. Breithaupt, C. Vidal, and R. Gould. *Drone Impact Assessment on Aircraft Structure: Windshield and Leading Edge Testing and Analysis*. Volume 2 of 2, 2020 doi: 10.4224/40001907.

18. Mohagheghian, I., Y. Wang, J. Zhou, L. Yu, X. Guo, Y. Yan, M. N. Charalambides, and J. P. Dear. Deformation and Damage Mechanisms of Laminated Glass Windows Subjected to High Velocity Soft Impact. *International Journal of Solids and Structures*, Vol. 109, 2017, pp. 46–62 doi: 10.1016/j.ijsolstr.2017.01.006.

19. Mohagheghian, I., M. N. Charalambides, Y. Wang, L. Jiang, X. Zhang, Y. Yan, A. J. Kinloch, and J. P. Dear. Effect of the Polymer Interlayer on the High-Velocity Soft Impact Response of Laminated Glass Plates. *International Journal of Impact Engineering*, Vol. 120, 2018, pp. 150–170 doi: 10.1016/j.ijimpeng.2018.06.002.

20. Ritt, S. A., and L. Bühler. *Evaluation of Material Alternatives for Rotorcraft Canopies Under Drone Versus Bird Strike,* Wichita, 20-23.06.2023.

21. Bühler, L., S. A. Ritt, and N. Toso. Drone and Bird Strike on a Polycarbonate Helicopter Windshield. *Ansys Innovation Conference*, 2024.

22. Siemann, M. H., and S. A. Ritt. Novel Particle Distributions for SPH Bird-Strike Simulations. *Computer Methods in Applied Mechanics and*

Engineering, Vol. 343, 2019, pp. 746–766 doi: 10.1016/j.cma.2018.08.044.

23. Dantec Dynamics. *FlexDIC.* https://www.dantecdynamics.com/solutions/digital-image-correlation-dic/flexdic/. Accessed July 10, 2025.
24. Jones, E., M. Iadicola, R. Bigger, B. Blaysat, C. Boo, M. Grewer, J. Hu, A. Jones, M. Klein, P. Lava, M. Pankow, K. Raghavan, P. Reu, T. Schmidt, T. Siebert, M. Simonsen, A. Trim, D. Turner, A. Vieira, and T. Weikert. *A Good Practices Guide for Digital Image Correlation*, 2018 doi: 10.32720/idics/gpg.ed1/print.format.